



Open Archive Toulouse Archive Ouverte

OATAO is an open access repository that collects the work of Toulouse researchers and makes it freely available over the web where possible

This is an author's version published in: <https://oatao.univ-toulouse.fr/26619>

Official URL :

<https://doi.org/10.1002/cphc.201700693>

To cite this version:

Jońca, Justyna and Ryzhikov, Andrey and Palussière, Ségolène and Esvan, Jérôme and Fajerweg, Katia and Menini, Philippe and Kahn, Myrtil L. and Fau, Pierre *Organometallic Synthesis of CuO Nanoparticles: Application in Low-Temperature CO Detection*. (2017) ChemPhysChem, 18 (19). 2658-2665. ISSN 1439-4235

Any correspondence concerning this service should be sent to the repository administrator: tech-oatao@listes-diff.inp-toulouse.fr

Organometallic Synthesis of CuO Nanoparticles: Application in Low-Temperature CO Detection

Justyna Jońca,^[a] Andrey Ryzhikov,^[a] Ségolène Palussière,^[a] Jérôme Esvan,^[d]
Katia Fajerweg,^[a, b] Philippe Menini,^[c] Myrtil L. Kahn,^{*[a]} and Pierre Fau^{*[a, b]}

A metal–organic approach has been employed for the preparation of anisotropic CuO nanoparticles. These nanostructures have been characterized by transmission and high resolution transmission electron microscopy, field-emission scanning electron microscopy, X-ray powder diffraction, Fourier transform infrared spectroscopy and X-ray photoelectron spectroscopy. The CuO nanoparticles have been deposited as gas-sensitive layers

on miniaturized silicon devices. At an operating temperature of 210 °C, the sensors present an optimum response toward carbon monoxide correlated with a fast response (R_n) and short recovery time. A high sensitivity to CO ($R_n \approx 150\%$, 100 ppm CO, RH 50%) is achieved. These CuO nanoparticles serve as a very promising sensing layer for the fabrication of selective CO gas sensors working at a low temperature.

1. Introduction

Despite intense research work in the field of metal oxide semiconductor (MOS) sensors, the need for highly sensitive and low-working-temperature gas-sensing devices remains a challenge. Different materials and sensor designs are used in order to improve these parameters. Several approaches have included: 1) the use of metal oxide nanoparticles with well controlled morphology and crystallinity,^[1] 2) the use of catalytic filters,^[2] 3) the functionalization of sensing layers with noble metals,^[3] and 4) the use of different heating temperatures, or various operating modes of the sensors.^[4]

n-type semiconducting oxides have been the focus of most of the research activities in the gas-sensing domain, whereas relatively few studies have been reported on p-type metal oxide gas sensors.^[5] Among them, copper II oxide (CuO), used

pure or in combination with n-type semiconducting oxide (p–n heterojunction), has demonstrated considerable potential for detection of gases, such as C₃H₈, C₂H₅OH, NO₂, H₂S, H₂, CO, NH₃ and HCN.^[6] CuO nanowires structures were used by Kim et al.^[6c] and Steinhauer and co-workers^[7] for CO detection at an optimized temperature of 300 °C. Up to now, various approaches have been used to fabricate the CuO nanostructures, such as solid-state reaction processes,^[8] a sol–gel method,^[6a, 9] hydrothermal method,^[6f, 10] thermal oxidation method,^[6c, 7] electrochemical method,^[11] template methods using carbon nanotubes^[12] or sonochemical method.^[6b] In this paper, we describe a metal–organic chemistry approach for the synthesis of small CuO nanoparticles. This method is based on the hydrolysis of N,N'-diisopropylacetamidinato copper I (CuAmd) in the presence of an alkylamine ligand (octylamine, OA). As compared to many other methods, where high temperatures and/or pressure are required, the preparation of these nanoparticles has been done at room temperature and under atmospheric pressure which allows the formation of small size nanoparticles. This unique one-pot reaction does not require any special apparatus, such as autoclave, which is currently used in other methods.^[10b] The as-prepared nanoparticles have been deposited as gas sensitive layers on dedicated silicon platforms. The sensors properties to CO detection has been measured. Thanks to the small CuO nanostructures, an optimized response toward CO has been obtained at very low operation temperature (ca. 210 °C) which opens the way for the preparation of low consumption devices for portable applications.

2. Results and Discussion

Over the past 15 years, we developed a one-pot metalorganic approach for the preparation of metal oxide nanoparticles.^[13] This method is based on the controlled hydrolysis of an organometallic precursor in an organic solvent in the presence of

[a] Dr. J. Jońca, Dr. A. Ryzhikov, S. Palussière, Dr. K. Fajerweg, Dr. M. L. Kahn, Dr. P. Fau

Laboratoire de Chimie de Coordination (LCC)
CNRS, 205 route de Narbonne
31077 Toulouse Cedex 4 (France)
E-mail: myrtil.kahn@lcc-toulouse.fr
pierre.fau@lcc-toulouse.fr

[b] Dr. K. Fajerweg, Dr. P. Fau
Université Paul Sabatier, UT III
118 route de Narbonne
31062 Toulouse Cedex 9 (France)

[c] Dr. P. Menini
Laboratoire d'Analyse et d'Architecture des Systèmes (LAAS)
CNRS, 5 avenue du Colonel Roche
31400 Toulouse (France)

[d] Dr. J. Esvan
CIRIMAT-ENSIACET, INP-ENSIACET
4 allée Emile Monso
31030 Toulouse (France)

Supporting Information and the ORCID identification number(s) for the author(s) of this article can be found under:
<https://doi.org/10.1002/cphc.201700693>.

stabilizing agent (typically alkyl amine or fatty carboxylic acid species), at room temperature and under ambient atmosphere. Indeed, the hydrolysis of the metalorganic precursor is so exothermic that well crystallized nanoparticles of controlled size and shape are obtained straightforward. This method has been used to achieve zinc oxide,^[13b,14] iron oxide^[15] and tin oxide nanoparticles.^[16] Here, for the first time, this approach is applied for the preparation of copper oxide nanoparticles. In this case, $[\text{Cu}(\text{iPr-Me-amd})]_2$ precursor is exposed to ambient atmosphere in the presence of octylamine (OA). In these conditions, a black powder spontaneously forms.

2.1. PXRD, TEM and HRTEM Analyses

Powder X-ray diffraction (PXRD) patterns reveal a monoclinic symmetry (space group $C2/c$, ICDD: 96-410-5683) characteristic of the CuO tenorite structure (Figure 1). Determination of the crystallite size using Scherrer equation gives values of ca. 4–5 nm while TEM images show the formation of rather anisotropic nanoparticles of larger size (Figure 2a).

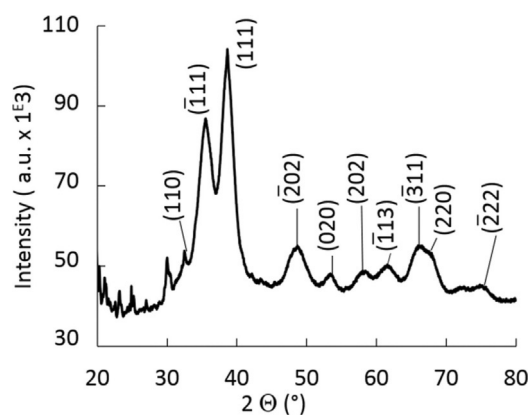


Figure 1. X-ray diffraction pattern of CuO powder.

High-resolution images clearly reveal different sets of lattice planes inside the particles (Figure 2b). The distances measured from Fourier transformation of the HRTEM image are $d=0.18$, 0.23, 0.25 and 0.27 nm, within the accuracy of the measurements. These distances are in very good agreement with the (20–2), (111), (11–1), and (110) interplanes distances anticipated for perfect monoclinic CuO (0.186, 0.252 and 0.275 nm, respectively). Interestingly, this HRTEM analysis reveals that the CuO nanorods are formed by aggregation of several nanocrystallites, suggesting a growth process driven by oriented attachment mechanism.^[17]

Analysis of the nanorods through a recently described 2D-plot representation^[18] leads to evidence three populations of different size (Figures 3). The first one possesses an average width of 4.6 ± 1.5 nm and length of 6.8 ± 2.7 nm and accounts for 50% of the population. The correlation between the length and the width is strong (0.42). The second population possesses an average width of 5.8 ± 2.3 nm and length of 8.9 ± 3.5 nm and accounts for 43%. In this case, the correlation between

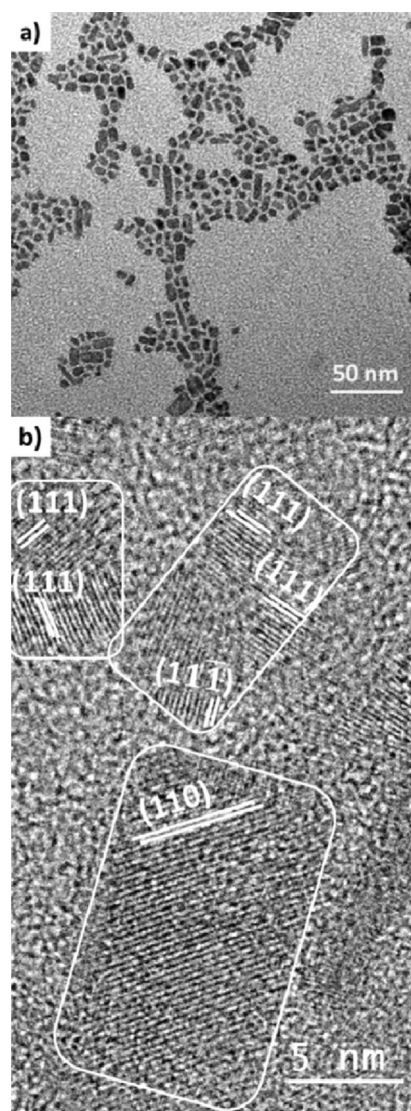


Figure 2. a) TEM images of as prepared CuO nanoparticles and b) HRTEM image of nanocrystals.

the length and the width is not evidenced (0.03). Finally, the third population, accounting for 6%, presents an average width of 6.5 ± 4.4 nm and length of 15.1 ± 10.0 nm with a correlation between the length and the width (0.22).

2.2. FTIR and XPS Analyses

FTIR spectra of various samples are shown on Figure 4. It is noteworthy that the elimination of the excess of ligand (OA), a prerequisite for best gas detection properties, is performed with acetone (see experimental part). Surprisingly, bands characteristic of carbamate species are observed on the FTIR spectra of as-prepared powder sample (Figure 4b), and these bands are still present after washing steps, even if their intensity is less intense compared to the as-prepared sample (Figure 4c).

In this study the carbamate species results from the spontaneous reaction of atmospheric CO_2 with OA in humid atmos-

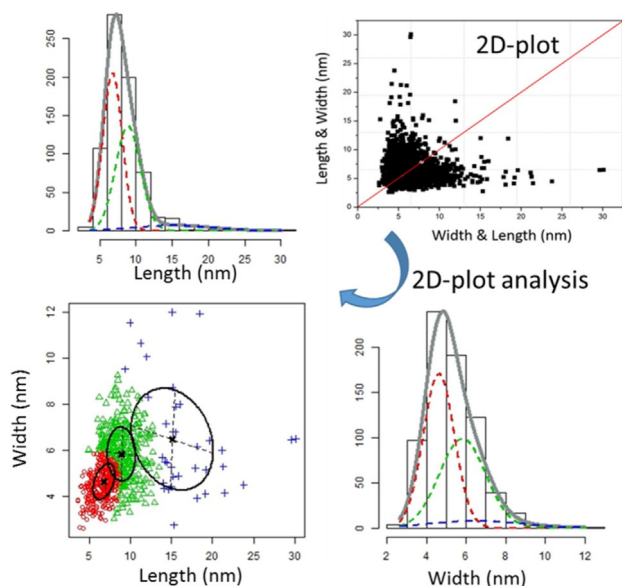


Figure 3. 2D plot analysis of CuO nanoparticles size showing three different populations.

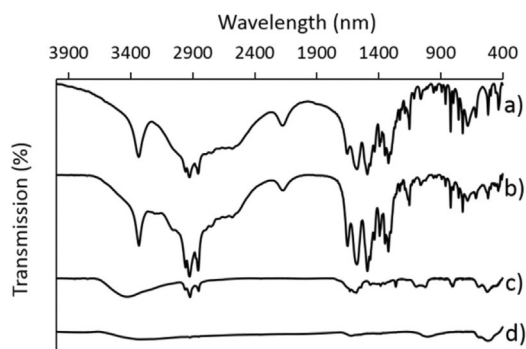


Figure 4. FTIR spectra of organic ligands and CuO powders according to different preparations: a) carbamate, b) as-prepared CuO c) CuO after washing steps d), CuO annealed at 450 °C.

phere. This is consistent with the results already observed by McCann et al.^[19] TGA analyses evidenced that around 50% of the organic species remain after the washing procedure (Figure S1). This is in contrast to what we reported in the case of the synthesis of SnO₂ nanoparticles stabilized with HDA (hexadecylamine) for which the same washing procedure was very efficient.^[16] Moreover, no carbamate species was observed in the case of the synthesis of SnO₂ by a similar method where the FTIR spectra only revealed the presence of the amine ligand.^[16] This result suggests that the formation of carbamate species is favoured in the case of CuO compared to SnO₂. These differences could be attributed to the more basic character of CuO compared with SnO₂.

On Figure 4 c and d the shoulder at 590 cm⁻¹ and the peak at ca. 530 cm⁻¹ are characteristic of Cu-O stretching in accordance with the XRD analysis showing CuO structure. The broad band centred at ca. 3320 cm⁻¹ can be assigned to O-H stretching band of water (Figure 4c). The IR signature of the CuO

samples after the washing and the in situ heating at 450 °C is consistent with the XPS analysis of C 1s, N 1s, O 1s and Cu 2p core level spectra (Figure 5). Indeed, the relative amount of C and N associated to organic species strongly decreased (not

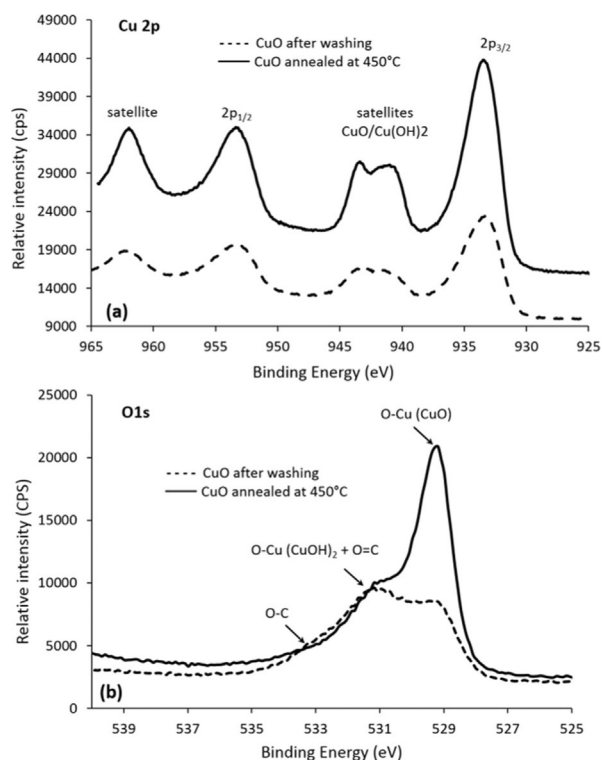


Figure 5. XPS core level spectra of the CuO samples: a) Cu 2p and b) O 1s.

shown). The residual organic species can be efficiently removed by an in situ heating of the sensitive layer up to 450 °C.

The chemical environment of CuO samples obtained after washing steps and washing plus annealing at 450 °C is shown in Figures 5a and 5b. Peaks at 933.4 eV and 933.8 eV reveal the presence of, respectively CuO and Cu(OH)₂ which confirms the oxidation state II of Cu species.^[20] They are accompanied by two satellite bands located at higher binding energy (B.E) (939–945 eV). The quantification and the fitting of core level spectra of O 1s (Figures S2a,b) confirm the presence of O in CuO (ca. 529 eV),^[21] in organic species (B.E range 933–935 eV) and in an intermediate component corresponding to a mixture of Cu(OH)₂ and CuO. The ratio CuO/Cu(OH)₂ = 1 (Figure S2a) and 3 (Figure S2b) clearly demonstrates that the presence of CuO is dominant. This result is confirmed by the CuL₃M_{4,5} M_{4,5} Auger signals (Figure S3).

2.3. ¹H NMR Analysis

Room temperature [D₈]toluene ¹H NMR spectra of dried supernatant obtained from the first washing step with acetone of the pristine CuO nanoparticles is presented Figure 6. The resonance of α(CH₂) and β(CH₂) protons of OA moiety is characterized by multiplets centred at δ = 3.14 and 1.64 ppm, respec-

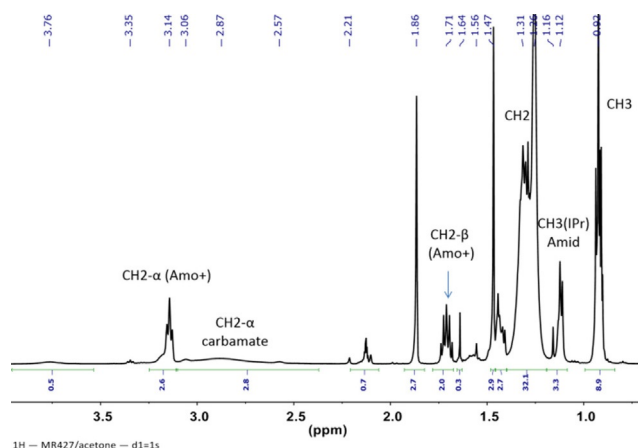
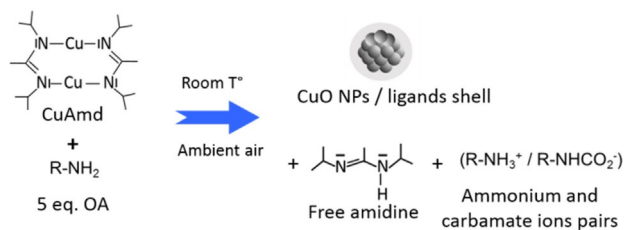


Figure 6. ^1H NMR spectrum of the supernatant obtained from the first washing step of CuO nanoparticles in $[\text{D}_8]\text{toluene}$.

tively, CH_3 end-group resonance is located at $\delta = 0.92$ ppm and resonance of the alkene protons is located at $\delta = 1.31$ ppm. The position of α and β (CH_2) signals presents a strong chemical shift characteristic of an ammonium (RNH_3^+) species rather than the amine molecules. The $\alpha(\text{CH}_2)$ protons of possible carbamate species, a counter ion associated to the ammonium moiety, is evidenced by the large signal at 2.87 ppm. Signals located at 1.16 ppm and 3.8 ppm may correspond, respectively to (CH_3) and (CH) of the isopropyl part of free amidine resulting from the hydrolysis of the copper precursor.

Such result is in agreement with the one reported by Makhoulfi et al. on the hydrolytic decomposition of metal amidinates showing the formation of *N*-(1-(dimethyl-14-azanylidene)ethyl)propan-2-amine molecule.^[22] In the former case, two independent molecules are asymmetrically connected through hydrogen bonds between two nitrogen atoms of the structure. Similarly, it is supposed that copper amidinate hydrolysis may give rise to free amidine compounds. These amidine species could be not in interaction with CuO nanoparticles. The presence of ammonium species is obvious from the NMR characterization and carbamate species are evidenced by FTIR spectra. In addition, it is proved that ions pair ligands and especially anionic carbamate ligands, possess a much higher stabilization capacity to nanocrystals compared to neutral ligands.^[23] Based on the analysis of FTIR spectra, NMR results and bibliographic evidences, we propose hereafter the most probable reaction Scheme of CuAmd in ambient air (Scheme 1).



Scheme 1. Reaction scheme of copper amidinate with OA under ambient air conditions and the resulting formation of CuO nanoparticles.

Thanks to the high reactivity of CuAmd compound to ambient air condition, the Cu–N bond is readily broken at room temperature and numerous coppers oxide germs appear in the reaction medium whilst Cu I oxidizes into Cu II. The reaction medium contains a high quantity of stabilizing agents since the reaction is driven in pure OA. A ligand shell composed of ionic pairs spontaneously binds on the CuO germs thanks to their good affinity on CuO nanocrystals. The ligand shell rapidly stops the particle growth up to few nanometres, leading to polycrystalline nanorods.

2.4. Response of CuO to CO Gas

The CuO nanoparticles have been deposited by an inkjet method (Microdrop AG) as gas sensitive layers on silicon gas sensing devices (Figure 7, top). After deposition, homogeneous

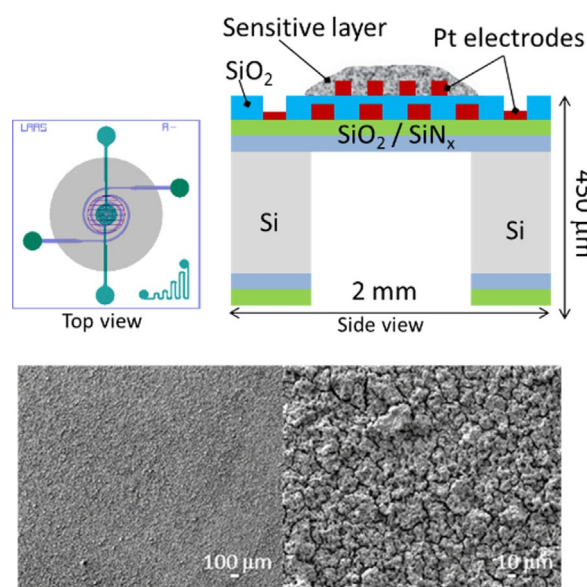


Figure 7. Schematic illustration of the silicon chip used for gas sensing analysis (top) and SEM images of the CuO layer on the gas sensor device (bottom). Top left: The platinum heater meander and the interdigitated sensing electrodes. Top right: Cross-section showing the different layers and membrane thickness (1.4 microns).

and micron thick layers are obtained as observed by SEM-FEG (Figure 7, bottom)

The normalized response (R_n , see Experimental Section) of the sensors to 100 ppm CO for various temperatures (150°C – 400°C) at relative humidity (RH) of 50% is presented Figure 8.

The gas sensing mechanism in MOS gas sensors is based resistance change of the sensitive layer, which results from charge transfer induced by surface reactions with the gas to be detected. The conductivity of p-type semiconducting oxides is driven by hole accumulation regime due to copper atoms deficiency in the structure. At the working temperature of the sensor, the adsorption and dissociation of oxygen (O^- species) on the oxide surface generate an accumulation of ma-

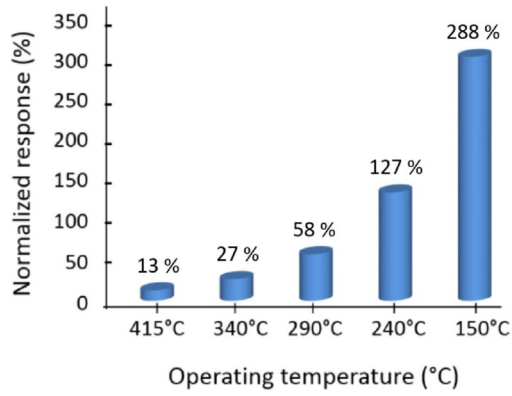


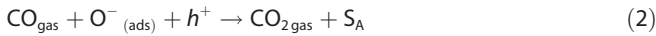
Figure 8. Normalized responses of CuO sensors to 100 ppm CO at different operating temperatures (RH 50%).

majority carriers and lower the electrical resistance of the sensor [Eq. (1)]:^[24]



Where $O_{2\text{air}}$ represents an O_2 molecule from air, S_A an adsorption site for oxygen, $O^-_{(\text{ads})}$ the chemisorbed oxygen ion and h^+ the hole in the valence band.

Reversibly, the adsorption and oxidation of a reducing gas as CO on the surface will react with the adsorbed oxygen ions and generate electrons that recombine with holes in the valence band as follows [Eq. (2)]:



The net result of CO adsorption is the increase of the resistance of CuO sensors. As the reaction of the surface species largely determine the change in resistance, the gas sensing performance of a metal oxide sensor is closely related to the morphology, size and surface chemistry of sensing materials.^[1a]

The working temperature has a major effect on the gas response of the sensors. Interestingly, the sensors response increases continuously when the temperature decreases (down to the lowest experimental value of 150 °C; Figure 8). This evolution with temperature is in contrast with the usual behaviour observed with n-type semiconducting oxides like SnO_2 where higher working temperature (above 250 °C) are correlated with optimum sensitivities.^[25] The surface of SnO_2 has to present a high number of adsorbed oxygen ions and must be free from undesired adsorbed species (water molecules, OH groups) in order to maximize CO adsorption sites. In addition, the low temperature CO response of our CuO sensors suggests that adsorption/desorption kinetics of CO molecules are of prime importance in the sensor sensitivity. From the previous results, we deduce that nanosized CuO grains present the highest density of adsorbed oxygen ions at low working temperatures. CO adsorption properties on CuO structures have been studied in the research field of catalytic properties of CuO. Avgouropoulos and Ioannides have shown by temperature-programmed techniques (TPD) that the interaction of CO with

CuO was found to be maximum for low reaction temperature (< 150 °C).^[26] CO reacts with adsorbed oxygen to release CO_2 at the maximum rate for temperatures close to 108–118 °C. This measurement corroborates our experimental results where the highest sensor reactivity appears at the lowest working temperature.

In order to optimize the operating temperature of sensors for the determination of an improved sensor response, a narrower temperature domain, between 110 °C and 240 °C, has been evaluated. Within this temperature range, sensors response still exhibits a large increase when temperature drops (Figure 9 and Table 1).

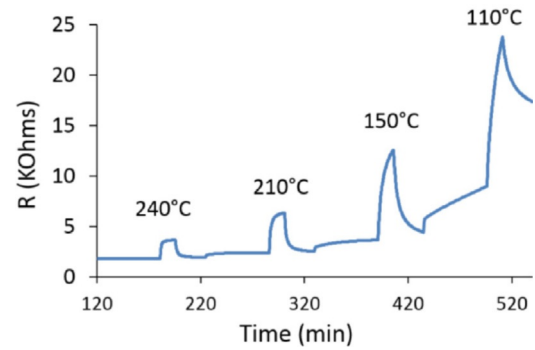


Figure 9. CuO sensors response to 100 ppm CO at different low operation temperatures (relative humidity, RH: 50%).

T [°C]	240	210	150	110
Normalized response [%]	127	146	288 ^[a]	164 ^[a]
Response time	2 s	4 s	> 15 min	> 15 min
Recovery time	12 s	19 s	> 15 min	> 15 min

[a] The gas response presents a very slow response time and the normalized response is measured before the complete resistance variation, this value is therefore a transitory one and is under-evaluated.

However, beside the response level, it is also necessary to take into account the effects of the operation temperature on the reaction kinetics occurring at the sensor surface. Indeed, response and recovery times are strongly affected by this parameter. At 240 °C, gas response is the lowest of the series (127%) but the response time of sensors is very fast with only 2 seconds required to reach 90% of the resistance variation (Table 1).

At 210 °C, gas response is improved (146%) while the dynamic of the sensors is still rapid (4 s to 90% resistance variation). When operating temperature decreases to 150 °C, gas response is even higher but this effect is detrimental to sensors kinetics. In this case, the resistance plateau under 100 ppm CO is not achieved even after 15 min of gas exposure and the recovery time is even longer since the baseline resistance is far from recovering the initial level even after 30 min of stabilization under air. This effect can be related to the blockage of

active sites by Cu^+ -CO carbonyls and/or by the formation of hydroxyl groups formed at low temperatures.^[27]

At 110 °C sensors resistance is not stabilized as shown by the drift of baseline resistance under humid air. However, at such low temperature, adsorption/desorption kinetics of gaseous molecules on the sensitive layer surface are considerably slowed down and long response time and incomplete recovery of the sensor make it unusable for practical application. The best balance between optimized sensor response and short kinetics is achieved around 210 °C. This temperature was therefore employed for all the other experimental tests under gas. It is noteworthy that such an optimal operation temperature is low compared to the ones reported in the literature which usually ranges between 250 to 300 °C. In addition, a strong sensitivity decrease is usually observed for temperature below 200 °C.^[6c,1,21,28] The very small size of the CuO grain reported here may account for such a low temperature response toward CO. The grain size of CuO sensors is as small as 7 nm (for ca. 50% of the total population) which is far beyond the Debye length for CuO of 12.7 nm.^[6c] The hole accumulation regime therefore extends from the surface to the inner part of the grains. This conditions induces a high reactivity of the whole grains of the sensitive layer which insures a large resistance change to the adsorption of gases.

The influence of humidity on sensors response toward 100 ppm CO has been investigated (Figure 10).

The devices exhibit high and rather stable sensitivity at humidity levels comprised between 30–90% (Rn ca. 140–150%). Slightly lower performance are observed for humidity level of 10% (Rn ca. 110%). To sum up, these sensors can work in a

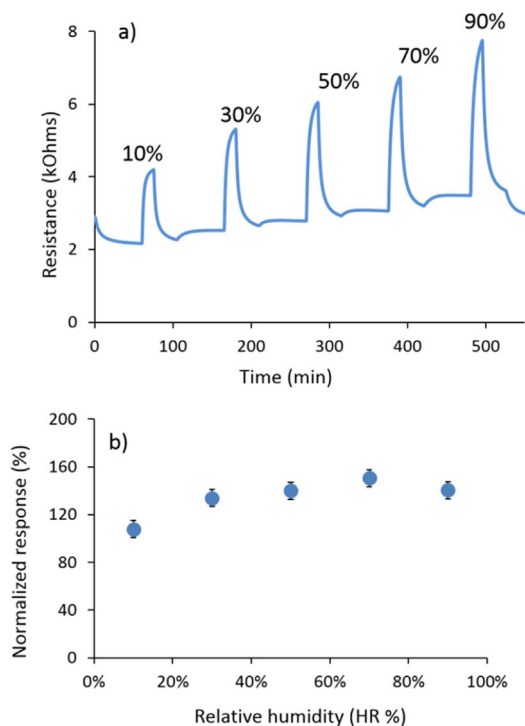


Figure 10. Response of CuO sensors to 100 ppm CO at different humidity levels (10–90%) and at an operating temperature of 210 °C, showing: a) resistance variation b) normalized response.

large concentration and humidity range and are characterized by a very low electrical resistance of about few kOhms (ca. 2–5 kOhms) which make them a perfect candidate for highly efficient CO sensing devices.

The sensors' responses have been evaluated after one month of storage in ambient air (Figure 11).

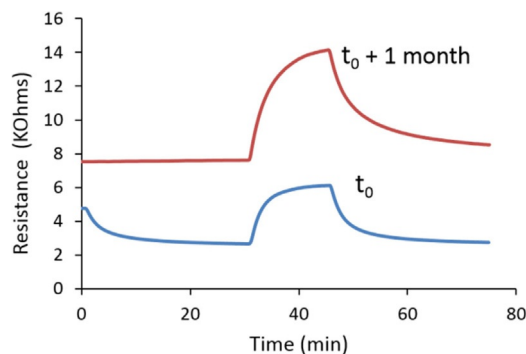


Figure 11. Stability test of CuO sensors after 1 month storage at room temperature.

An increase of the baseline resistance (from ca. 3 to 8 kOhms) of the sensors is observed at the working temperature of 210 °C. In addition, the sensors exhibit a decrease of 34% of the response to 100 ppm CO as well as much longer reaction and recovery times (Table 2).

Table 2. Response of the sensors to 100 ppm CO (210 °C, 50% RH) before and after storage for 1 month at room temperature.		
sensor	Initial test	Test after 1 month
Normalized response [%]	130	85
Response time [s]	7	10
Recovery time [s]	9	13

The high reactivity of nanosized CuO grains to ambient atmosphere may be responsible for such an undesired evolution. CuO is known to easily transform into copper carbonates or hydroxyl carbonates by simple air exposure over time.^[29] As an example, malachite ($\text{Cu}_2(\text{OH})_2\text{CO}_3$) or azurite ($\text{Cu}_3(\text{OH})_2(\text{CO}_3)_2$) are commonly observed when copper oxide is exposed to ambient air. However, copper carbonate are known to decompose at moderate temperatures^[30] (around 290 °C) and tenorite structure can be restored by the application of dedicated temperature steps above 300 °C. In the case of nanosized grains where the small grain volume is involved to the gas response, a chemical transformation of the surface will have a drastic effect on the sensing performances. Further studies focusing on surface species of the CuO grains surface with storage time in air will have to be performed in order to improve the overall performance of the CuO gas sensor.

3. Conclusions

The metalorganic approach described here is a powerful and simple one-pot synthesis method for the preparation of CuO nanostructures dedicated to sensitive gas sensors. Ambient air and room temperature decomposition of copper amidinate precursor in the presence of alkylamines (OA) generates ligands that favour an efficient stabilization effect for nanosized metal oxides. Small size and rather anisotropic nanostructures have been obtained presenting width and length being 4.6–6.8 nm (50% of the population) and 5.8–8.9 nm (43%) respectively. Gas sensors on silicon chips have been prepared by drop deposition technique of the CuO colloidal suspension and CO responses have been measured. Optimized CO sensitivities (146% resistance variation) and short response and recovery times (4 and 19 s, respectively) have been obtained at low operation temperature (ca. 210 °C). Such performances are fully compatible with the fabrication of very low consumption portable devices. However, after moderate storage time (1 month), the gas sensors show a noticeable decrease of their sensing performance (-34% of normalized response to CO). This undesired effect may be due to the high surface reactivity of the nanostructured oxide coupled with uncomplete recovery of the copper oxide surface operating at low temperature (210 °C).

Further studies dedicated to the study of surface chemistry of CuO grains and their thermal stability will have to be done in order to achieve functional gas sensors.

Experimental Section

Synthesis and Washing Protocol

Reactions have been performed at room temperature under an ambient atmosphere. (*N,N'*-diisopropylacetamidinato) copper (I), [Cu(*i*Pr-Me-amd)]₂ (NanoMePS, France) is used as the metalorganic precursor. Octylamine (Sigma Aldrich) is used as the stabilizing agent. In a typical experiment, [Cu(*i*Pr-Me-AMD)]₂ (0.125 mmol, 51 mg) is mixed with octylamine (0.625 mmol, 80.5 mg, 5 equiv.) and exposed to ambient atmosphere. After 16 h, the obtained black product is washed three times with 5 mL of acetone (Sigma Aldrich) using a centrifuge (5000 rpm, 20 °C, 5 min).

Characterization

A JEOL JSM 1011 Transmission Electron Microscope operating at 100 kV or a JEOL JSM 2100F High Resolution Transmission Electron Microscope operating at 200 kV were used for TEM or HRTEM imaging, respectively. Analysis of the images were performed using Digital Micrograph program. Field Emission Scanning Electron Microscopy (FESEM) images were obtained using JSM-6700F microscope operating at 10 kV. The powder-diffraction patterns have been obtained using SEIFERT XRD 3000 TT X-Ray Diffractometer with Cu-K α radiation, fitted with a diffracted-beam graphite monochromator. The data were collected in the 2 θ configuration between 20 and 80°. Fourier transformed infrared (FTIR) spectra were recorded in transmission mode on a PerkinElmer 100 spectrometer with KBr as the diluting agent. X-ray photoelectron spectroscopy (XPS) analysis was performed using a Thermoelectron Kalpha device. The photoelectron emission spectra were recorded using

Al-K α radiation ($h\nu=1486.6$ eV) from a monochromatized source. The X spot size was 400 μm . The pass energy was fixed at 40 eV for narrow scans (and 150 eV for the survey). We used Flood Gun for the charge effects. The spectrometer energy calibration was made using the Au 4f^{7/2} (83.9 \pm 0.2 eV) and Cu 2p^{3/2} (932.8 \pm 0.2 eV) photoelectron lines. XPS spectra were recorded in direct N(Ec). The background signal was removed using the Shirley method. The binding energy scale was established by referencing the C 1s value of adventitious carbon (284.6 eV). The photoelectron peaks were analyzed by Lorentzian/Gaussian (L/G=30) peak fitting. Thermogravimetric analysis (TGA) were performed using a Setaram 92-16.18 Thermobalance with a ramp of 10 °C min⁻¹, in the 30–500 °C range under ambient air.

Sensor Preparation

The as-prepared CuO powders were dispersed in ethanol (Sigma Aldrich), using ultrasound treatment (45 kHz, 10 min), at a concentration of 5 mg mL⁻¹. The mixture was drop-deposited on miniaturized gas sensors substrates by a semi-manual ink-jet method (Autodrop AD system, Microdrop AG, Germany). The silicon platforms were developed by the Laboratoire d'Etudes et d'Architecture des Systèmes, LAAS-CNRS in the MICA group. The die size is 2 \times 2 mm, and integrates a 1.4 μm thick dielectric membrane (SiN_x/SiO₂) designed for an optimized thermal insulation of the heated zone. A platinum heater, designed with a spiral shape, is buried between the bottom dielectric membranes and a passivation silicon dioxide top layer. This heater structure stands a temperature up to 700 °C, and the power consumption is 55 mW at a working temperature of 500 °C. The sensitive layer resistance is measured by interdigitated platinum electrodes which are deposited on the SiO₂ passivation layer. A distance of 10 μm between each electrode pole provides a reliable contact with the sensing layers.^[1a]

Gas Test Set-Up

Gas tests have been performed using a PC controlled setup composed of different gas bottles connected to mass flow controllers (QualiFlow) commanded by an Agilent Data Acquisition/Switch Unit 34970A. Sensors are placed in a measurement cell equipped with humidity and temperature sensors. The integrated heaters are commanded by a HP6642A tension controller. The National Instruments 6035E electronic card establishes the connection between the computing unit and the measurement cell. Freshly prepared sensors are firstly conditioned by a sequential in situ heating of the sensitive layer up to 450 °C in ambient air. Afterwards, the sensors are stabilized by heating of the layer at 450 °C in synthetic air (RH 50%) at a total gas flow rate of 1 L.min⁻¹. Finally, the sensors are exposed to various levels of CO at different operating temperatures. Resistance is measured before and after sensor exposure to reducing gas and the normalized response (Rn %) is calculated as the resistance variations, that is, $R_n (\%) = |(R_{\text{air}} - R_{\text{gas}})/R_{\text{air}} * 100|$, where R_{air} corresponds to the sensor resistance in synthetic air and R_{gas} corresponds to the sensor resistance in the reducing gas mixture. The response time is the time to reach 90% of the maximum resistance variation after injection of the reacting gas and the recovery time corresponds to a sensor resistance value 10% above the baseline resistance value measured under air.

Acknowledgements

The work was financially supported by BPI France in the frame of the Object's World project. We thank our partners Sigfox and Alpha-M.O.S. SA. We would like to thank Dr. Laure Vendier for X-ray diffraction analysis, Vincent Collière for HRTEM microscopy and Dr. Yannick Coppel and Dr. Christian Bijani for NMR studies. We are grateful to CNRS and Université de Toulouse, Toulouse III Paul Sabatier for their support.

Conflict of interest

The authors declare no conflict of interest.

Keywords: CO detection • CuO nanoparticles • gas sensors • organometallic synthesis • p-type metal oxides

- [1] a) A. Ryzhikov, J. Jonca, M. Kahn, K. Fajerweg, B. Chaudret, A. Chapelle, P. Menini, C. H. Shim, A. Gaudon, P. Fau, *J. Nanopart. Res.* **2015**, *17*, 1–10; b) D. Chen, X. Hou, T. Li, L. Yin, B. Fan, H. Wang, X. Li, H. Xu, H. Lu, R. Zhang, J. Sun, *Sens. Actuators B* **2011**, *153*, 373–381.
- [2] a) J. Jońca, J. Harmel, L. Joanny, A. Ryzhikov, M. L. Kahn, P. Fau, B. Chaudret, K. Fajerweg, *Sens. Actuators B* **2017**, *249*, 357–363; b) C. O. Park, S. A. Akbar, J. Hwang, *Mater. Chem. Phys.* **2002**, *75*, 56–60.
- [3] a) J. Guo, J. Zhang, M. Zhu, D. Ju, H. Xu, B. Cao, *Sens. Actuators B* **2014**, *199*, 339–345; b) S. N. Olliaee, A. Khodadadi, Y. Mortazavi, S. Alipour, *Sens. Actuators B* **2010**, *147*, 400–405.
- [4] A. Heilig, N. Barsan, U. Weimar, M. Schweizer-Berberich, J. W. Gardner, W. Gopel, *Sens. Actuators B* **1997**, *43*, 45–51.
- [5] A. S. Zoofakar, R. Abdul Rani, A. J. Morfa, A. P. O'Mullane, K. Kalantar-zadeh, *J. Mater. Chem. C* **2014**, *2*, 5247–5270.
- [6] a) M. Breedon, S. Zhuiykov, N. Miura, *Mater. Lett.* **2012**, *82*, 51–53; b) Y.-J. Chen, F.-n. Meng, H.-I. Yu, C.-I. Zhu, T.-s. Wang, P. Gao, Q. — y. Ouyang, *Sens. Actuators B* **2013**, *176*, 15–21; c) J.-H. Kim, A. Katoch, S.-W. Choi, S. S. Kim, *Sens. Actuators B* **2015**, *212*, 190–195; d) A. Rydosz, A. Szkudlarek, *Sensors* **2015**, *15*, 20069–20085; e) D. P. Volanti, A. A. Felix, M. O. Orlandi, G. Whitfield, D.-J. Yang, E. Longo, H. L. Tuller, J. A. Varela, *Adv. Funct. Mater.* **2013**, *23*, 1759–1766; f) L. Wang, Y. Kang, Y. Wang, B. Zhu, S. Zhang, W. Huang, S. Wang, *Mater. Sci. Eng. C* **2012**, *32*, 2079–2085; g) M. Yang, J. He, X. Hu, C. Yan, Z. Cheng, Y. Zhao, G. Zuo, *Sens. Actuators B* **2011**, *155*, 692–698; h) Y.-B. Zhang, J. Yin, L. Li, L.-X. Zhang, L.-J. Bie, *Sens. Actuators B* **2014**, *202*, 500–507; i) A. I. Ayes, A. F. S. Abuhani, S. T. Mahmoud, Y. Haik, *Sens. Actuators B* **2016**, *231*, 593–600; j) L. Li, Y. Hu, D. Deng, H. Song, Y. Lv, *Anal. Bioanal. Chem.* **2016**, *408*, 8831–8841; k) G. Peng, S. Wu, J. E. Ellis, X. Xu, G. Xu, C. Yu, A. Star, *J. Mater. Chem. C* **2016**, *4*, 6575–6580; l) F. Wang, H. Li, Z. Yuan, Y. Sun, F. Chang, H. Deng, L. Xie, H. Li, *RSC Adv.* **2016**, *6*, 79343–79349; m) A. S. Zoofakar, M. Z. Ahmad, R. Abdul Rani, J. Z. Ou, S. Balendhran, S. Zhuiykov, K. Latham, W. Wlodarski, K. Kalantar-zadeh, *Sens. Actuators B* **2013**, *185*, 620–627.
- [7] S. Steinhauer, V. Singh, C. Cassidy, C. Gspan, W. Grogger, M. Sowwan, A. Koeck, *Nanotechnology* **2015**, *26*, 1–6.
- [8] S. Sohrabnezhad, A. Valipour, *Spectrochim. Acta Part A* **2013**, *114*, 298–302.
- [9] I. Singh, R. K. Bedi, *Appl. Surf. Sci.* **2011**, *257*, 7592–7599.
- [10] a) N. Datta, N. Ramgir, M. Kaur, S. Kailasa Ganapathi, A. K. Debnath, D. K. Aswal, S. K. Gupta, *Sens. Actuators B* **2012**, *166–167*, 394–401; b) T. Jiang, Y. Wang, D. Meng, X. Wu, J. Wang, J. Chen, *Appl. Surf. Sci.* **2014**, *311*, 602–608; c) D. Wang, C. Song, X. Lv, Y. Wang, *Appl. Phys. A* **2016**, *122*, 1–10; d) Y. Wang, T. Jiang, D. Meng, J. Yang, Y. Li, Q. Ma, J. Han, *Appl. Surf. Sci.* **2014**, *317*, 414–421.
- [11] B. Tobaosung, P. Singjai, *J. Alloys Compd.* **2011**, *509*, 4132–4137.
- [12] W. Li, N. D. Hoa, D. Kim, *Sens. Actuators B* **2010**, *149*, 184–188.
- [13] a) M. L. Kahn, A. Glaria, C. Pages, M. Monge, L. Saint Macary, A. Maisonnat, B. Chaudret, *J. Mater. Chem.* **2009**, *19*, 4044–4060; b) J. Rubio-Garcia, Y. Coppel, P. Lecante, C. Mingotaud, B. Chaudret, F. Gauffre, M. L. Kahn, *Chem. Commun.* **2011**, *47*, 988–990.
- [14] a) M. L. Kahn, M. Monge, V. Colliere, F. Senocq, A. Maisonnat, B. Chaudret, *Adv. Funct. Mater.* **2005**, *15*, 458–468; b) M. Monge, M. L. Kahn, A. Maisonnat, B. Chaudret, *Angew. Chem. Int. Ed.* **2003**, *42*, 5321–5324; *Angew. Chem.* **2003**, *115*, 5479–5482; c) S. Saliba, Y. Coppel, M.-F. Achard, C. Mingotaud, J.-D. Marty, M. L. Kahn, *Angew. Chem. Int. Ed.* **2011**, *50*, 12032–12035; *Angew. Chem.* **2011**, *123*, 12238–12241.
- [15] a) A. Glaria, M. L. Kahn, P. Lecante, B. Barbara, B. Chaudret, *ChemPhys-Chem* **2008**, *9*, 776–780; b) A. Glaria, M. L. Kahn, A. Falqui, P. Lecante, V. Collière, M. Respaud, B. Chaudret, *ChemPhysChem* **2008**, *9*, 2035–2041.
- [16] J. Jońca, A. Ryzhikov, M. L. Kahn, K. Fajerweg, A. Chapelle, P. Menini, P. Fau, *Chem. Eur. J.* **2016**, *22*, 10127–10135.
- [17] Q. Zhang, S.-J. Liu, S.-H. Yu, *J. Mater. Chem.* **2009**, *19*, 191–207.
- [18] Z. Zhao, Z. Zheng, C. Roux, C. Delmas, J.-D. Marty, M. L. Kahn, C. Mingo-taud, *Chem. Eur. J.* **2016**, *22*, 12424–12429.
- [19] N. McCann, D. Phan, X. Wang, W. Conway, R. Burns, M. Attalla, G. Puxty, M. Maeder, *J. Phys. Chem. A* **2009**, *113*, 5022–5029.
- [20] a) R. P. Vasquez, *Surf. Sci. Spectra* **1998**, *5*, 262–266; b) R. P. Vasquez, *Surf. Sci. Spectra* **1998**, *5*, 267–272.
- [21] A. Klinbumrung, T. Thongtem, S. Thongtem, *Appl. Surf. Sci.* **2014**, *313*, 640–646.
- [22] G. Makhloufi, K. Schuette, C. Janiak, *Z. Kristallogr. New Cryst. Struct.* **2014**, *229*, 429–430.
- [23] P. E. Chen, N. C. Anderson, Z. M. Norman, J. S. Owen, *J. Am. Chem. Soc.* **2017**, *139*, 3227–3236.
- [24] "Conduction mechanism in semiconducting metal oxide sensing films: impact on transduction", N. Barsan, M. Huebner, U. Weimar in *Semiconductor gas sensors*, Woodhead Publishing Series in Electronic and Optical Materials (Eds. R. Jaaniso, O. K. Tan), **2013**, pp. 35–63.
- [25] L. Yu, X. Fan, L. Qi, L. Ma, W. Yan, *Appl. Surf. Sci.* **2011**, *257*, 3140–3144.
- [26] G. Avgouropoulos, T. Ioannides, *Catal. Lett.* **2007**, *116*, 15–22.
- [27] a) K. Hadjiivanov, H. Knozinger, A. Milushev, *Catal. Commun.* **2002**, *3*, 37–44; b) T. Kida, T. Kuroiwa, M. Yuasa, K. Shimanoe, N. Yamazoe, *Sens. Actuators B* **2008**, *134*, 928–933.
- [28] F. Yang, J. Guo, M. Liu, S. Yu, N. Yan, J. Li, Z. Guo, *J. Mater. Chem. A* **2015**, *3*, 20477–20481.
- [29] N. B. Tanvir, O. Yurchenko, C. Wilbertz, G. Urban, *J. Mater. Chem. A* **2016**, *4*, 5294–5302.
- [30] G. A. El-Shobaky, A. S. Ahmad, A. N. Al-Noaimi, H. G. El-Shobaky, *J. Therm. Anal.* **1996**, *46*, 1801–1808.